Structure
Article

Structure of the Mammalian 80S Ribosome at 8.7 Å Resolution

Preethi Chandramouli,[1] Maya Topf,[2,5] Jean-François Ménétret,[1,5] Narayanan Eswar,[3,5] Jamie J. Cannone,[4] Robin R. Gutell,[4] Andrej Sali,[3] and Christopher W. Akey[1,*]
[1]Department of Physiology and Biophysics, Boston University School of Medicine, 700 Albany Street, Boston, MA 02118, USA
[2]School of Crystallography, Birkbeck College, University of London, Malet Street, London WC1E 7HX, United Kingdom
[3]Department of Biopharmaceutical Sciences, California Institute for Quantitative Biomedical Research, QB3 at Mission Bay, University of California, San Francisco, 1700 4th Street, San Francisco, CA 94158, USA
[4]The Institute for Cellular and Molecular Biology, The University of Texas at Austin, Austin, TX 78712, USA
[5]These authors contributed equally to this work.
*Correspondence: cakey@bu.edu
DOI 10.1016/j.str.2008.01.007

SUMMARY

In this paper, we present a structure of the mammalian ribosome determined at ~8.7 Å resolution by electron cryomicroscopy and single-particle methods. A model of the ribosome was created by docking homology models of subunit rRNAs and conserved proteins into the density map. We then modeled expansion segments in the subunit rRNAs and found unclaimed density for ~20 proteins. In general, many conserved proteins and novel proteins interact with expansion segments to form an integrated framework that may stabilize the mature ribosome. Our structure provides a snapshot of the mammalian ribosome at the beginning of translation and lends support to current models in which large movements of the small subunit and L1 stalk occur during tRNA translocation. Finally, details are presented for intersubunit bridges that are specific to the eukaryotic ribosome. We suggest that these bridges may help reset the conformation of the ribosome to prepare for the next cycle of chain elongation.

INTRODUCTION

The cytoplasmic ribosome is a signature component of free-living cells. This machine is composed of small and large subunits, which work together to translate proteins from mRNAs with the aide of cognate amino-acylated tRNAs and additional factors (Green and Noller, 1997; Ramakrishnan, 2002). Recent crystal structures of the bacterial small subunit have provided insights into the decoding center and the basis of translational fidelity (Wimberly et al., 2000; Schluenzen et al., 2000; Pioletti et al., 2001; Carter et al., 2000; Brodersen et al., 2000; Ogle et al., 2001; Ogle and Ramakrishnan, 2005). Similarly, structures of large subunits from bacteria and archaea have revealed the architecture of the peptidyl transferase center, the L1 stalk, the exit tunnel, and a universal docking surface for factors that interact with the nascent polypeptide chain (Ban et al., 2000; Harms et al., 2001). In the 70S ribosome, the relative positions of the small and large subunits and the role of the intersubunit bridges have also been documented (Yusupov et al., 2001; Korostelev et al., 2006; Selmer et al., 2006; Schuwirth et al., 2005). In addition, structures of programmed bacterial ribosomes have defined a path for the translocation of mRNA and tRNAs through the intersubunit space (Yusupova et al., 2001, 2006; Korostelev et al., 2006; Selmer et al., 2006; Berk et al., 2006).

Peptide bond formation lies at the heart of translation and is catalyzed by rRNA (Schmeing et al., 2005; Jenni and Ban, 2003). During translation, the small subunit moves with a ratchet-like motion relative to the large subunit (Frank and Agrawal, 2000; Valle et al., 2003b). In addition, the head of the small subunit undergoes a swiveling motion that may be coupled with the translocation of tRNAs (Schuwirth et al., 2005; Berk et al., 2006; Spahn et al., 2004a). The translation cycle requires the sequential action of many factors that interact with the ribosome. Snapshots of these processes have provided insights into initiation (Allen et al., 2005), revealed the interactions of EF-Tu/amino-acylated tRNA with the ribosome (Frank et al., 2005; Valle et al., 2003a; Stark et al., 2002), and given details of EF-G-mediated translocation (Datta et al., 2005; Stark et al., 2000; Diaconu et al., 2005).

The larger yeast ribosome contains many novel proteins that are not found in bacterial ribosomes (Dresios et al., 2006). In addition, hypervariable inserts are present in the subunit rRNAs which are known as expansion segments (ES) (Gerbi, 1996; Schnare et al., 1996). Parallel studies on the *Saccharomyces cerevisiae* ribosome have also demonstrated a ratchet-like motion of the small subunit (Spahn et al., 2001, 2004a). In general, the translation cycle in eukaryotes is more complex than in prokaryotes, as additional regulatory steps are used to fine-tune this process (Ramakrishnan, 2002).

The mammalian ribosome is even larger than the yeast ribosome (Wool et al., 1995; Dresios et al., 2006). The size difference is due primarily to expansion segments in the large subunit rRNA, as mammalian and yeast ribosomes contain a similar number of proteins. The functions of the expansion segments are not well known, but at least one insert is required for cell viability (ES27; Sweeney et al., 1994). The added complexity of the eukaryotic ribosome is also reflected by the assembly of small and large subunits in the nucleolus. This process requires ~200 accessory proteins and numerous snoRNPs (Rudra and Warner, 2004; Fromont-Racine et al., 2003).

In this paper, we present a molecular model of the canine 80S ribosome with an E site tRNA that is based on a density map at ~8.7 Å resolution. This structure reveals the architecture of the eukaryotic ribosome, including expansion segments and

α-helical rods within novel proteins. We also show that RACK1, the receptor for activated protein kinase C, interacts with rRNA and a novel protein domain in the small subunit. Importantly, the conformation of the ribosome in our model is similar to bacterial ribosomes that contain P and E site tRNAs. Thus, our model depicts the mammalian ribosome at the "start" of the translation cycle. This structure also provides additional insight into the roles of the small subunit and L1 stalk during translation. Finally, our model suggests a role for intersubunit bridges that are specific to the eukaryotic ribosome. These bridges could help reset the conformation of the ribosome during the subunit ratcheting motion, to prepare for the next cycle of translation.

RESULTS

The Native Ribosome-Channel Complex

In this study, electron cryomicroscopy and single-particle image processing were used to obtain an improved, three-dimensional (3D) map of the canine ribosome-channel complex (RCC) (Ménétret et al., 2005; Ludtke et al., 1999; see the Supplemental Data available with this article online). In the map, the ribosome and the channel are at ~8.7 and ~24 Å resolution, respectively (Figure S1). A rotation series of the RCC is shown in Figure 1, with the small subunit in gold and the large subunit in blue. Many rods and spiral, ribbon-like features are present on the surface of the ribosome, which can be attributed to α helices and A form helices, respectively. The native channel (shown in magenta) binds to a flat docking surface on the bottom of the large subunit and is composed of Sec61 and the translocon-associated protein complex (TRAP; Ménétret et al., 2005). To further our understanding of the RCC, we have built a molecular model of the canine ribosome. We then focused our analysis on novel regions in the canine ribosome and evaluated models for movements of the small subunit and L1 stalk during translation.

Modeling Conserved Ribosomal RNA and Proteins

Our current model incorporates crystal structures of ribosomal RNAs from the small subunit of *Thermus thermophilus* (Wimberly et al., 2000), the large subunit of *Haloarcula marismortui* (Ban et al., 2000), and certain regions of the 70S ribosome (Korostelev et al., 2006; Selmer et al., 2006). Overall, the fit of the conserved subunit rRNAs within the map was excellent (see thin slabs through the ribosome in Figures S2A–S2D) and only a few RNA domains needed to be repositioned (Supplemental Data). The fit of A form helices in the map is shown in Figure S3A.

In the next step, comparative models for conserved proteins in the small and large subunits were docked in the map and refined with some manual adjustments (Supplemental Data; Topf et al., 2006, 2008). In total, we modeled 16 chains in the small subunit (including RACK1) and 32 chains in the large subunit (Tables S1 and S2). The protein models were validated by the correspondence between α helices and rod-like density in the map (Figure S3B). In addition, β sheets and some hairpins formed flattened densities at a suitable threshold which were used to position these features in the map (as shown for proteins L9e and L26e; Figure S3B). Final correlation values for the small and large subunits with all of the modeled components were 0.70 and 0.68, respectively.

Front and back views of the canine ribosome are shown in Figures 2A and 2C, with the modeled core rRNA and conserved proteins. The full pseudoatomic models are shown without the map in Figures 2B and 2D. For completeness, these figures include expansion segments (red), along with spherical markers and rods for the novel proteins (shown in red for the small subunit and green for the large subunit) and the E site tRNA. The overall fit can be judged by viewing interface views of the small and large subunits, as these regions are highly conserved (Figures S4A and S4B). Empty density at the periphery of the subunits arises from regions of the expansion segments and novel proteins that were not modeled explicitly. A rotation series of the small (Figure S5) and large subunits (Figure S6) shows the modeled eukaryotic proteins. Importantly, sequence comparisons of subunit rRNAs and conserved proteins show that canine and human ribosomes are virtually identical. Hence, our model should be representative of the human ribosome.

Expansion Segments

Hypervariable expansion segments in subunit rRNAs are responsible, in part, for the altered morphology of eukaryotic ribosomes relative to their prokaryotic cousins (Spahn et al., 2001, 2004b; Morgan et al., 2002; Dube et al., 1998). We found that many of these RNA inserts contain well-ordered A form helices. In the small subunit there are 11 expansion segments, and 6 of these segments were modeled as A form helices (Figure 3; Figure S7). However, the distal half of $ES3^S$ and a major part of $ES6^S$ are flexible and were not modeled. In the large subunit, there are 16 notable expansion segments (Figures S8A and S8B), and 6 of these hypervariable regions are much enlarged ($ES7^L$, 9^L, 15, 27, 30, and 39) relative to their yeast counterparts (Gerbi, 1996; Schnare et al., 1996). These 6 expansion segments account for a mass of ~0.4 MDa. In total, we modeled ~50% of the nucleotides in the expansion segments. The remaining regions extend into solution and are flexible or form nonhelical structures (Figure S9).

We found that $ES3^L$ and $ES4^L$ in the 5.8S rRNA form helices within a cluster of expansion segments that includes $ES5^L$, ES19, ES20, and ES31. This cluster is located on the side and bottom of the large subunit (Figures 3B and 3D). Notably, ES19 and ES31 form three helical segments, but the insertion points are too close together to allow an unambiguous identification of two of these helices (ES19/31 in Figure 3B). A massive expansion segment (ES27, 700 nt) originates on the lower surface of the large subunit and faces the small subunit, but is almost entirely disordered. However, a smaller ES27 in the yeast ribosome extends toward the tunnel exit and is displaced when Sec61 is bound (Beckmann et al., 2001). Together, ES27 and ES41 on the large subunit combine with $ES3^S$, $ES6^S$, and $ES12^S$ on the small subunit to form a region of negatively charged RNAs located at the subunit interface (Figures 3A, 3B, and 3D). This region also contains unmodeled flexible RNA from $ES3^S$, $ES6^S$, and ES27. We also found that $ES12^L$ forms a small extension from the central protuberance, adjacent to two small helices that may arise from $ES9^L$ and ES10 (Figure 3C; Figure S8A). In addition, a short segment (ES30) is largely disordered, but it could affect the binding of cellular factors to the L1 stalk.

Four major expansion segments form a tubular network on the back of the large subunit; this is composed of A form helices and a knot-like structure (Figure 3C; Figure S8). $ES7^L$ is the largest expansion segment (813 nt) and one branch, denoted ES7_1, radiates outward from its insertion point to form a protrusion

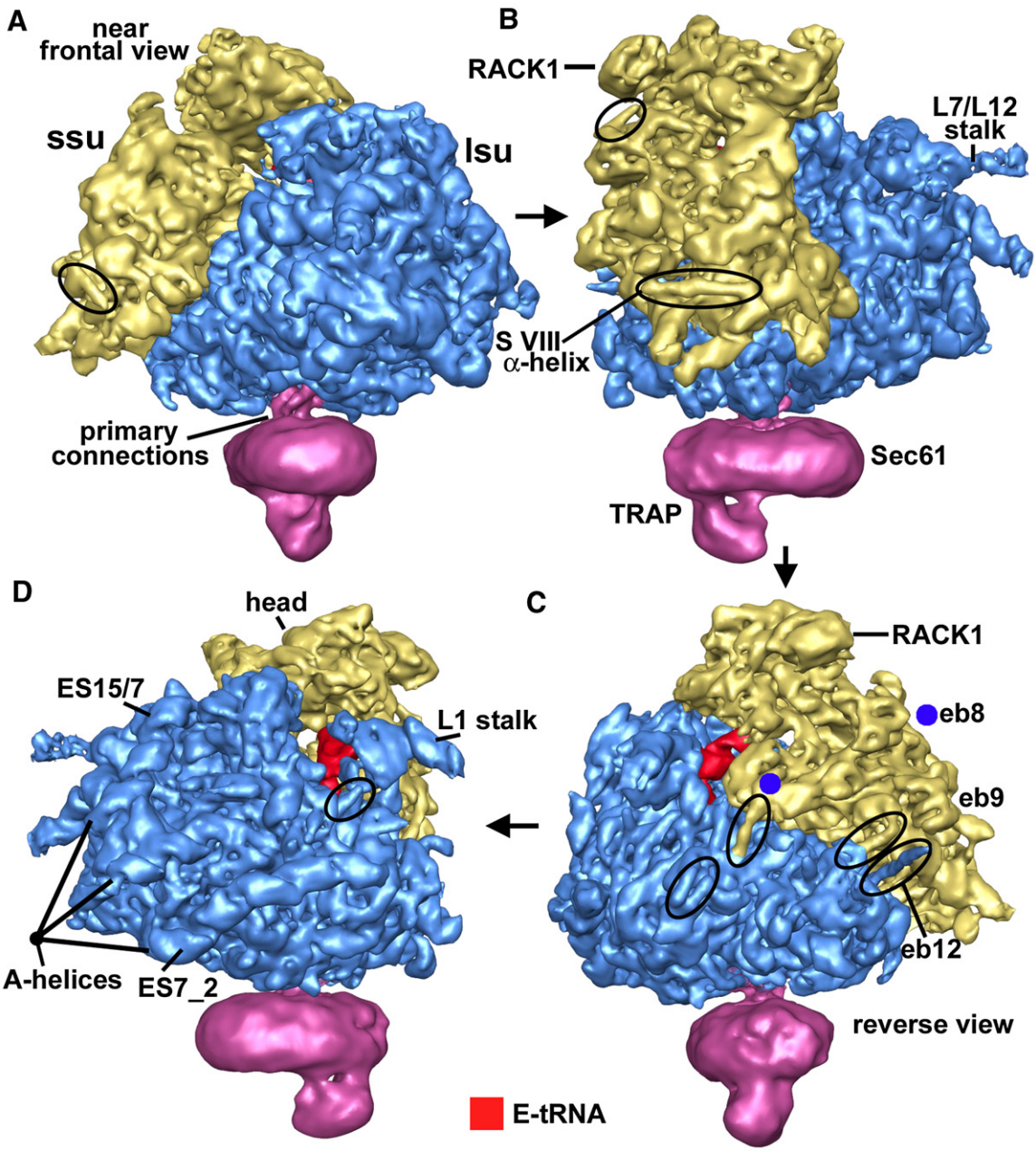

Figure 1. Surface Views of the Ribosome-Channel Complex

A rotation series is shown about a vertical axis for the RCC with the ribosome filtered at 8.7 Å resolution. Some protein α helices are outlined with ellipses in (A), (B), (C), and (D). The small subunit is shown in gold, the large subunit is in blue, and the native channel is in magenta. Some A form helices of expansion segment RNAs are marked in (D). The E site tRNA (red) is visible in (C) and (D) between the small and large subunits.

beneath the L7/L12 stalk. ES7^{L} also "merges" with ES9^{L} and ES15 to form the knot-like structure on the back of the large subunit (see dashed ring, labeled PK, in Figure 3C). A second branch of ES7^{L} (ES7_2) extends from the ES7^{L}/ES9^{L}/ES15 pseudoknot, wraps around the back of the large subunit, and becomes disordered near the L1 stalk. ES9^{L} starts near the pseudoknot (beneath ES12^{L}) and extends outward from the large subunit (Figure 3D). A prominent spine runs from the pseudoknot toward the central protuberance (CP) and may be formed by ES15. A lower branch also extends from the pseudoknot. Because ES7^{L} could account for one of these branches, both features are labeled "ES15/7." Finally, ES39 forms a group of four helices beneath ES7_1 and the L7/L12 stalk (Figure 3C).

Many of the expansion segments interact with conserved proteins or novel proteins (Table S3; see next section). In addition, conserved proteins that bind to expansion segments have acquired additional basic residues through which these interactions might be formed. In the case of L35e, a newly modeled, α-helical extension binds to ES5 (Figure 3D). Most of the conserved proteins that bind to expansion segments form links between the

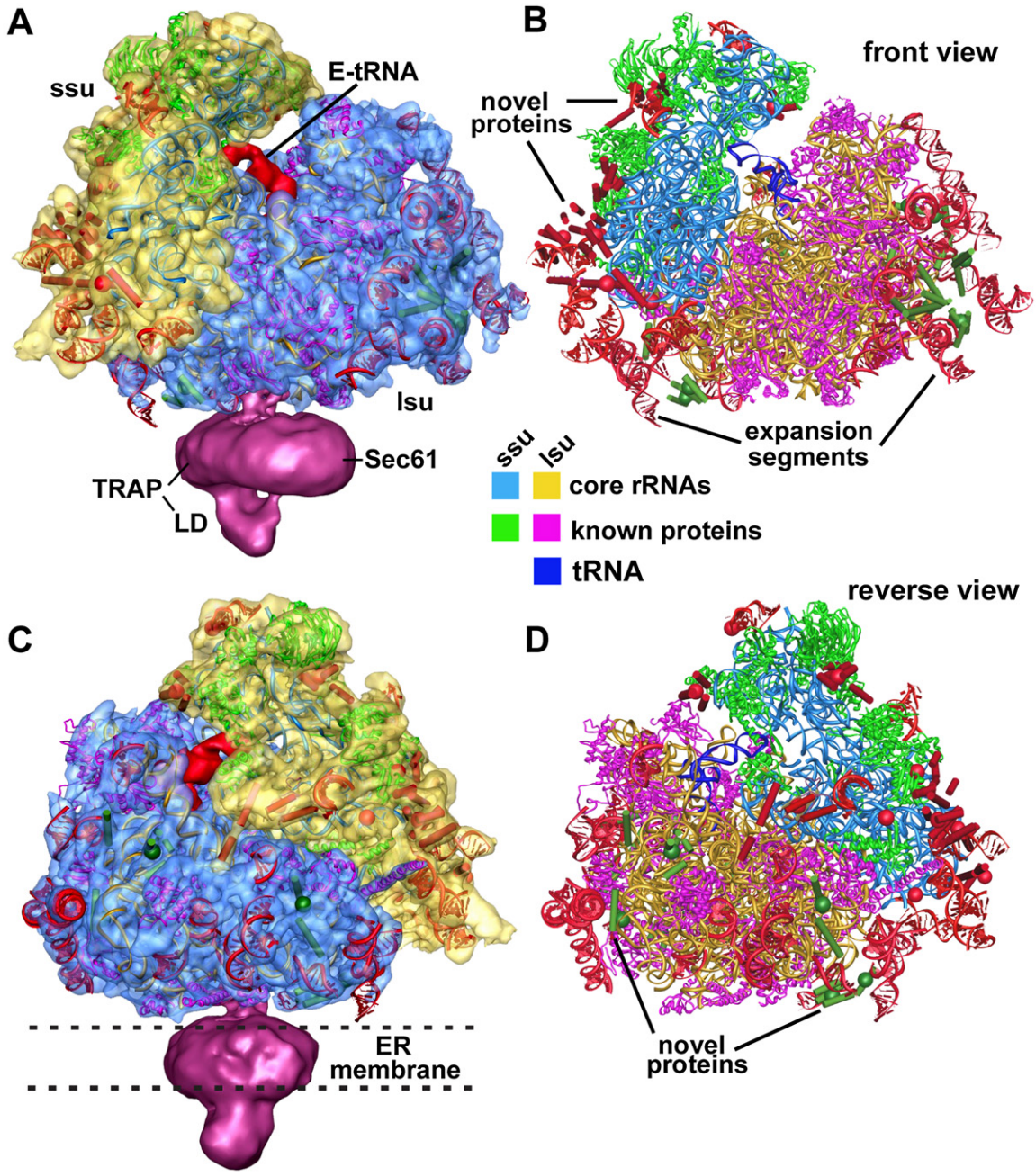

Figure 2. A Model of the Cytoplasmic 80S Ribosome

(A) A model of the canine ribosome is shown within a density map of the ribosome-channel complex. The E site tRNA is shown in red between the small (ssu) and large subunits (lsu) of the ribosome. This specimen contained part of the ER translocon (in magenta) that is composed of Sec61 and TRAP. The latter has a prominent lumenal domain (LD).

(B) A molecular model of the canine ribosome is shown in a front view. The subunit rRNAs and conserved proteins are color coded (see boxes). Novel proteins (spheres and rods) and expansion segments (red helices) are also included.

(C) The model of a canine ribosome is shown in a reverse view within the electron microscopy (EM) density map. The position of the ER membrane is indicated by dashed lines.

(D) The molecular model of the canine ribosome is shown in a reverse view.

subunit rRNA and the ES. These conserved proteins are shown with their expansion segment partners in Figure 3 and are colored yellow and blue in the small and large subunits, respectively. The overall effect of these protein-mediated interactions is to tether proximal regions of expansion segments to the ribosome, while leaving distal regions in solution. To interact with these extended rRNAs, hypothetical cellular proteins could recognize their secondary structure and/or negatively charged surfaces.

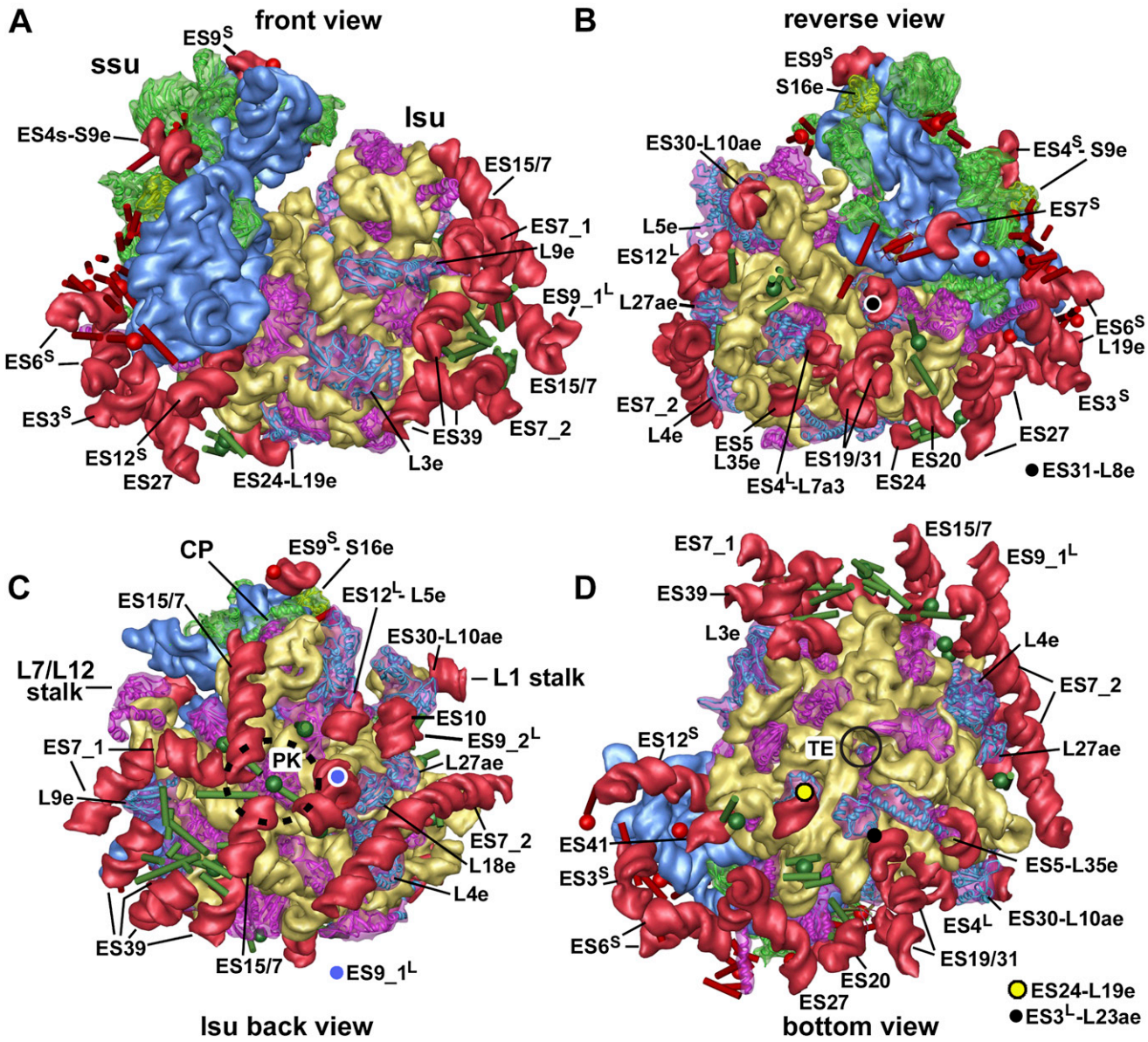

Figure 3. Expansion Segments and Interacting Proteins in the Canine Ribosome

(A) The model of the canine ribosome is shown in a front view with the ES depicted as red ribbons. The ssu and lsu rRNAs are shown as blue and gold ribbons, respectively. The conserved protein models are shown in green and magenta for the ssu and lsu. Proteins that interact with ES are colored yellow and blue and are labeled with their partner ES. The novel proteins are marked by spheres and modeled α helices are depicted as rods.

(B) A reverse view is shown of the model.

(C) A back view of the lsu reveals $ES7^L$ and ES15. The $ES7^L$/$ES9^L$/ES15 pseudoknot (PK) is marked by a dashed ellipse near the center of the lsu. Note that expansion segments with the same numerical designation in each subunit have a superscript (S or L) to identify them.

(D) A bottom view reveals the model as viewed from the ER membrane. The tunnel exit is marked with a circle (TE).

Novel Proteins

During evolution, 31 novel proteins have been added to the eukaryotic ribosome including 17 in the small subunit and 14 in the large subunit. However, only 20 unknown protein densities could be identified in our map, with 10 in each subunit (Table S4). A similar number of novel proteins were identified previously in the yeast ribosome at ~15 Å resolution (Spahn et al., 2001). In general, the positions of these proteins are conserved and this allowed us to adopt their nomenclature. Many of the novel proteins contain rod-like features that are probably α helices. In total, 56 of these rods were modeled as α helices in the small and large subunits. These modeled helices are shown as cylinders in the small and large subunits, along with spheres to mark the novel proteins (Figures 4A and 4B). These novel proteins are generally found on exposed surfaces of the subunits and 12 of the novel proteins appear to interact with expansion segments (Table S3).

For example, we identified a novel protein (S-VIII) in the small subunit that contains two long α-helical rods. This protein

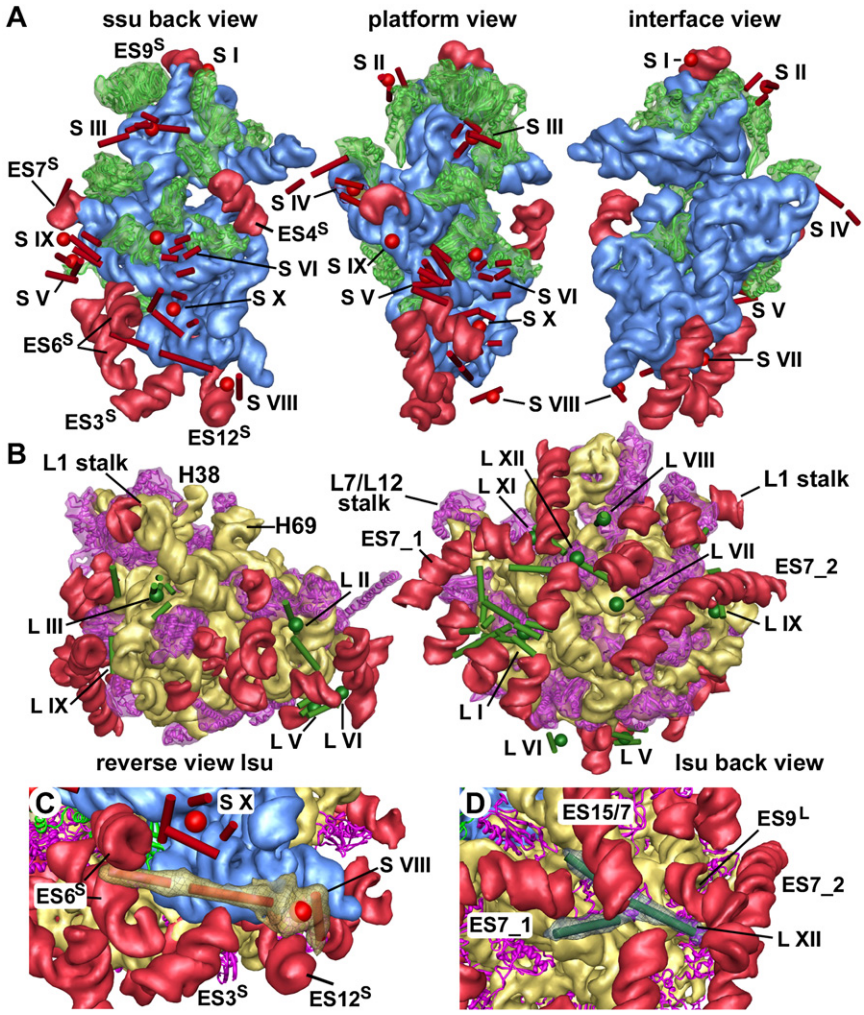

Figure 4. Novel Proteins in the Canine Ribosome

(A) Novel proteins of the ssu are marked with red spheres and possible α helices are indicated by red cylinders. The core rRNA and ES are shown as blue and red ribbons, and the conserved proteins are shown in green. The ssu is shown in back, platform, and interface views.

(B) Novel proteins in the lsu are marked with green spheres and cylinders for α helices. The core rRNA and ES are shown as gold and red ribbons and the conserved proteins are colored magenta. The lsu is shown in reverse and back views.

(C) Novel protein S-VIII is composed of two long rods between $ES3^S$, $ES6^S$, and $ES12^S$. This protein may also interact with $ES1^S$, which forms a bulge and has not been modeled.

(D) Density for novel protein L-XII reveals two long, intersecting α helices beneath the $ES7^L$/$ES9^L$/ES15 pseudoknot on the back of the lsu.

interacts with $ES6^S$ and $ES12^S$ by spanning the large distance between them (Figure 4C). Protein S-VIII may also interact with $ES3^S$. In addition, some unmodeled density between the rods (see red sphere, Figure 4C) may correspond to $ES1^S$, which forms a bulge, and some additional protein. In the large subunit, the L-XII protein density contains two long α helices (one of which is ~90 Å long) that intersect to form a "Y" (Figure 4D). These α helices underlie the large pseudoknot (Figure 3C) and may interact with $ES9\_1^L$, $ES15/7^L$, and $ES7^L\_1$. Hence, long α helices are used to link A form RNA helices in neighboring expansion segments and may stabilize the packing of these features against the core rRNA. Finally, a domain of the S-IV density contains α helices and β strands with an S6p-like configuration (see Intersubunit Bridges section). This similarity was verified by a local crosscorrelation which gave a value of 0.65. There is no known homolog of S6p in eukaryotes, but this domain of S-IV may be related to S6p. The similarity is striking because the S6p and S-IV proteins are each located near the platform in their respective small subunits. One domain of the S-IV density also links $ES7^S$ with the body of the small subunit and may form intersubunit bridge eb8 (see Intersubunit Bridges section).

The Exit Site and L1 Stalk

Transfer RNAs (tRNAs) are the adaptors that translate information encoded in mRNA into protein sequences. The ribosome in our map contains an exit site tRNA that may have originated from the displacement of a P site tRNA after puromycin treatment of programmed RCCs (Morgan et al., 2002). Electron density for the E site tRNA (Figures 5A–5C, shown in silver) reveals that its conformation and interactions are similar in mammalian and bacterial ribosomes (Selmer et al., 2006; Korostelev et al., 2006). Thus, the anticodon arm interacts with S5e, whereas the acceptor arm is near L44e (Figures 5A and 5B). The L1 stalk is flexible and may act as a lateral gate to release the E site tRNA (Gomez-Lorenzo et al., 2000; Harms et al., 2001; Valle et al., 2003b).

In our structure, the L1 stalk was modeled with H76–H78 from the *T. thermophilus* ribosome (Selmer et al., 2006). Based on the map, the D and T loops of the E site tRNA contact the N-terminal domain of L10ae and H76, respectively. In the yeast ribosome with bound eEF2 and sordarin (Spahn et al., 2004a), the L1 stalk adopts an inward conformation that partially blocks the canonical E site (blue stalk labeled Y, Figure 5C). However, the L1 stalk is displaced laterally when an E site tRNA is bound in mammalian (gold ribbon, Figure 5C) and bacterial ribosomes (see Selmer et al., 2006; Korostelev et al., 2006). Extensive contacts made by the E site tRNA imply that a significant conformational change of the L1 stalk is required to release the tRNA, as shown in the *Deinococcus radiodurans* large subunit (Figure 5C, red H76, labeled D; Harms et al., 2001) and also in the yeast ribosome (see Spahn et al., 2004a; Morgan et al., 2002). Interestingly, we observed a tubular density that links the body of the large subunit (near L27ae and protein L-IX) to protein L10ae on the L1 stalk (Figure 5D; Table S4). This density was modeled as an α helix,

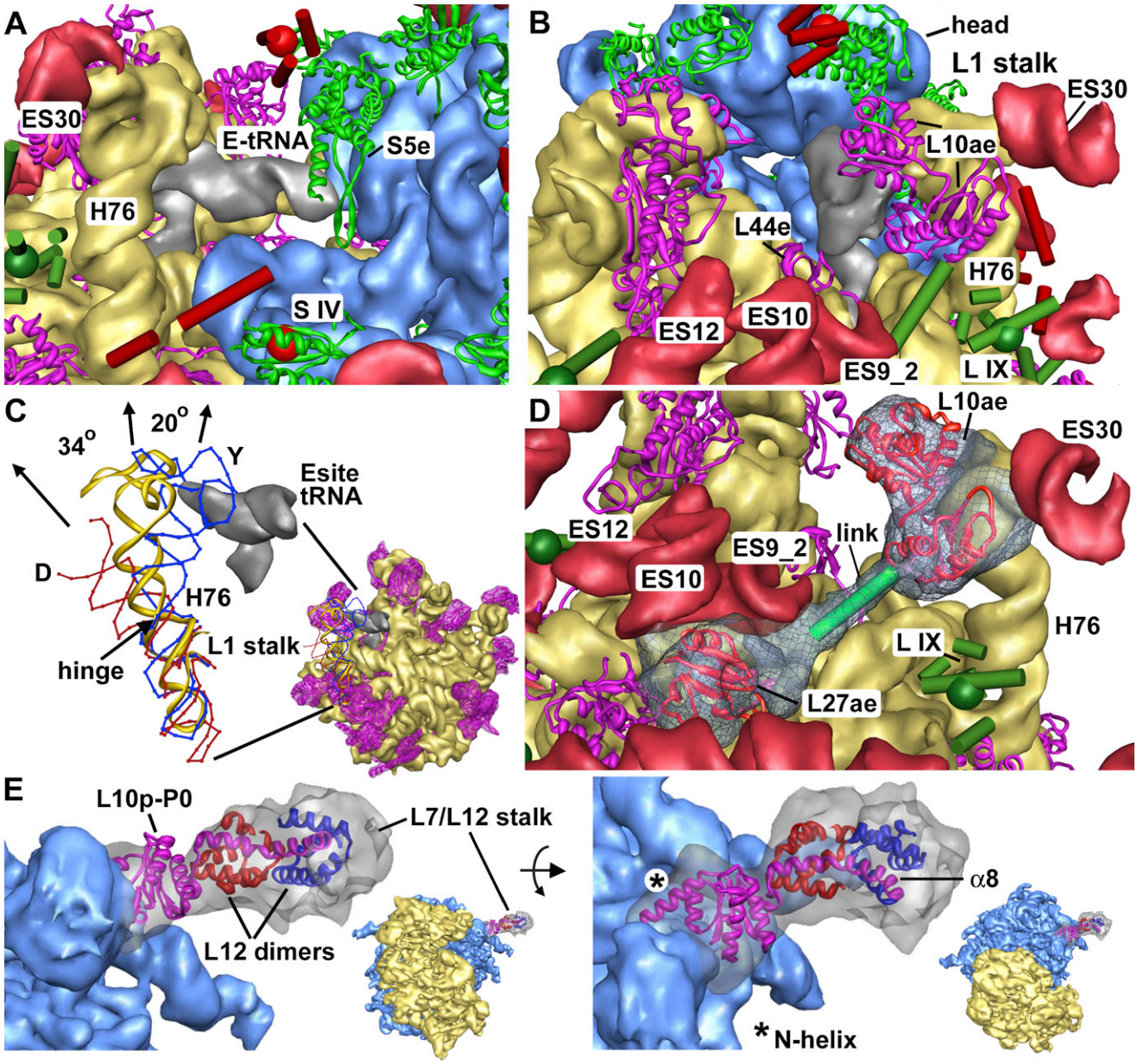

Figure 5. The E Site tRNA, L1 and L7/L12 Stalks

(A) Electron density for the E site tRNA (in silver) is shown in a reverse view in the canine ribosome model. The anticodon stem interacts with a β hairpin of S5e. The tRNA density was zoned out of the 3D map with Chimera (Goddard et al., 2005).

(B) The E site tRNA (in silver) interacts with L44e, L10ae, and the top of H76, as seen in an oblique top view of the ribosome.

(C) The L1 stalk may function as a lateral gate for the E site tRNA. L1 stalks are shown from a yeast ribosome with bound eEF2 and sordarin (Y) and from a *D. radiodurans* crystal structure (D) in blue and red, respectively. The L1 stalk in the canine ribosome with an E site tRNA is shown in gold and a possible hinge in H76 is marked.

(D) A rod-like density links L27ae on the body of the lsu and L10ae on the L1 stalk. These proteins have been colored in red and are shown in their electron density.

(E) The L7/L12 stalk is anchored by the N-terminal helix of L10p/P0 to the lsu (asterisk). This flexible stalk can contain two dimers of P1/P2 modeled here by L12p.

and it may be necessary to uncouple this link when the E site tRNA is released in mammalian ribosomes.

The L7/L12 Stalk

Little is known about the structure of the L7/L12 stalk in the mammalian ribosome. In bacteria, the L7/L12 stalk forms a remarkable machine that uses motions of flexibly linked, C-terminal domains of L7-L12 dimers to recruit EF-Tu, EF-G, and other factors to the ribosome (Diaconu et al., 2005). In different species, the L7/L12 stalk is composed of either four or six copies of the L7-L12 homologs. The N-terminal domains of the L7-L12 dimer bind to helix α8 of L10p to form an extended helix bundle in the stalk, and the number of bound dimers is proportional to the length of helix α8 (Diaconu et al., 2005). In eukaryotes, two

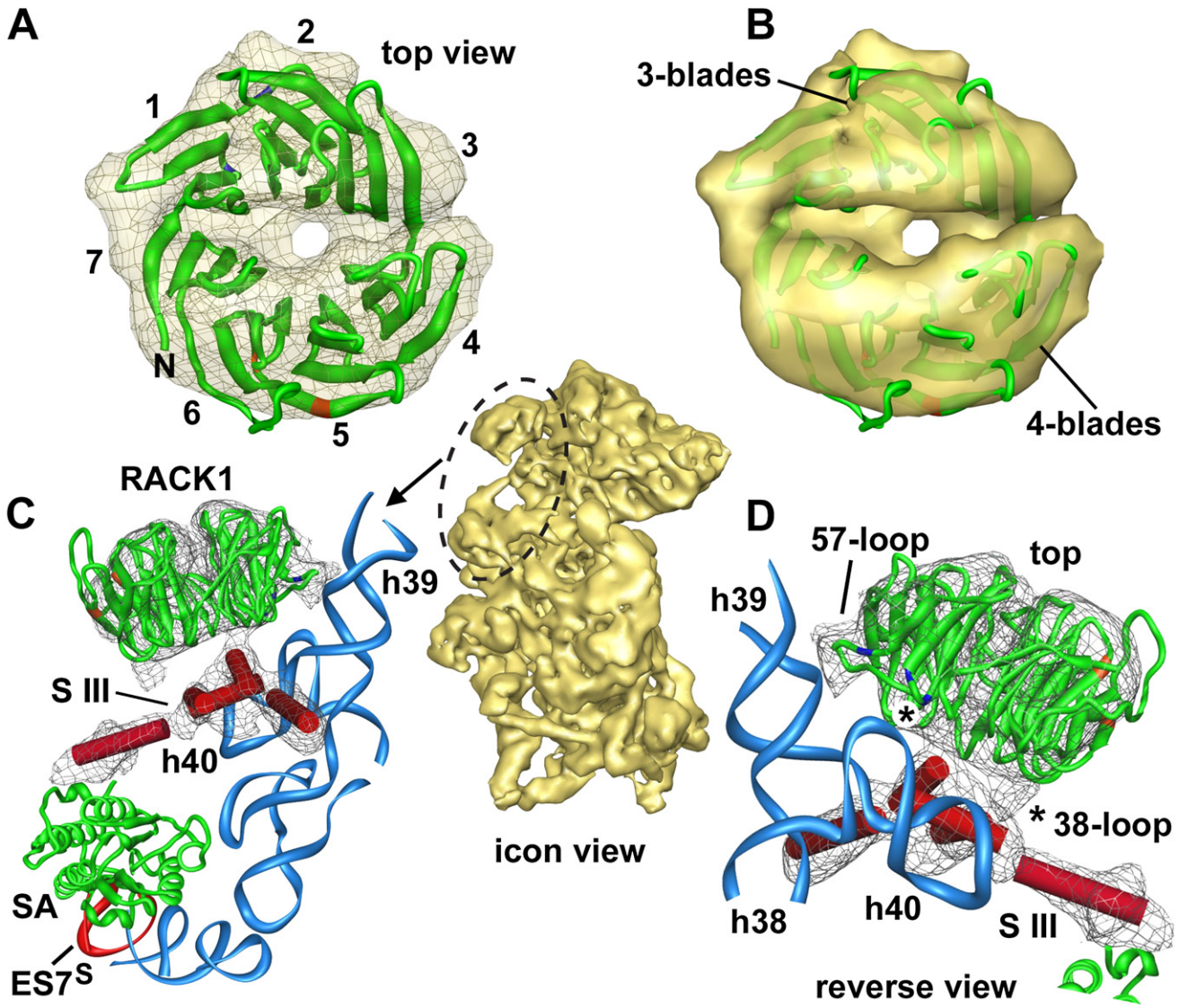

Figure 6. RACK1 Binding to the Small Subunit

(A) A top view of the RACK1 homology model (green ribbon) is shown in the EM density map (gray mesh) as viewed along the pseudo-7-fold axis. The blades of the β propeller are grouped into sets of three and four, respectively. Tyrosines that may interact with SRC kinase (Y229, Y247) are shown in red.

(B) A surface view of RACK1 shows the division into two halves with three and four blades.

(C) RACK1 interacts with h39 and a novel protein density (marked S-III). This view corresponds to the region circled in the central icon of the ssu. The EM map is shown in gray mesh.

(D) RACK1 is shown at higher magnification in a reverse view. Interactions are indicated between the 57-loop and h39 and between the 38-loop and h40. The S-III protein density may be an extension of SA/S0 and sits directly below RACK1.

copies of the L12p homologs, known as P1/P2, may be bound to the P0/L10p protein (Gonzalo and Reboud, 2003).

In our map, the L7/L12 stalk is present when the resolution is truncated to ~12 Å, but at ~8.7 Å resolution the distal region of the stalk is fragmented. This behavior results from an innate flexibility of the L7/L12 stalk (Figure S9, panel 3). We docked a model of the *Thermotoga maritima* L10-L12 complex with two L12p dimers into the map (Figure 5E; Diaconu et al., 2005). This docking was guided by the fit of the N-terminal helix of L10p/P0 into a well-resolved rod near H42 (not shown). We also introduced a slight bend in the complex to better fit the density. Although the fit is not perfect, the length of this feature is consistent with the idea that the mammalian L7/L12 stalk contains two dimers of P1/P2 bound to P0.

RACK1 Interactions with the Small Subunit

RACK1 is a conserved receptor for activated protein kinase C and forms a β propeller with seven WD40 repeats. The RACK1 protein has been identified on the small subunit of eukaryotic ribosomes where it is bound near the mRNA exit site (Figure 6, central icon; Sengupta et al., 2004). Thus, RACK1 may serve as a binding site for protein kinase C, which regulates the

initiation step of protein translation by phosphorylating eIF6 on the large subunit (Sengupta et al., 2004; Ceci et al., 2003). RACK1 may also direct ribosomes to focal adhesions for targeted translation (Nilsson et al., 2004).

In our study, a RACK1 homology model was created using a seven-bladed β propeller from the Protein Data Bank (PDB; see the Supplemental Data). When this model was docked into the map, we found that mammalian RACK1 is shifted outward a bit, relative to its position near h40 in the yeast ribosome (Sengupta et al., 2004). However, the rotational alignment of the β propeller on the small subunit is similar in the yeast and mammalian models (not shown). Intriguingly, we found that the RACK1 density is distorted by a lateral offset between opposing three- and four-blade segments of the β propeller (Figures 6A and 6B). One possible explanation for this asymmetry is that the RACK1 β propeller may be intrinsically distorted, as occurs in the clathrin heavy chain (ter Haar et al., 1998). In an alternate model, this distortion could have arisen from the binding of the first three blades to the small subunit. In this case, the outer four-blade region may be somewhat flexible and could move laterally along the line demarcated by the canyon-like feature between the two halves of the propeller (Figures 6A and 6B; Figure S10). Thus, the density map may reflect an intrinsic flexibility of RACK1 on the small subunit.

In any case, our docking placed RACK1 next to h39 and showed that this receptor interacts with a novel protein near h40 (Figure 6C). The interaction with h40 involves the "38-loop," which contains Arg36 and Lys38 (Figure 6D). Canine RACK1 also contains a loop with Arg57 that fits into the density and may interact with helix h39 (near nt 1121; Figure 6D). Thus, mammalian RACK1 makes distinct contacts with helices h39 and h40 using adjacent blades of the β propeller. In contrast, yeast RACK1 makes two contacts with h40 that involve the 36- and 280-loops (Sengupta et al., 2004). Yeast and human RACK1 share ~53% sequence identity, so their global folds should be similar. However, RACK1 interactions with rRNA may have been modified during ~1.5 billion years of divergent evolution.

RACK1 binding to the canine small subunit also involves a novel protein domain located beneath the β propeller (near h38 and h40; Figure 6D). Intriguingly, the adjacent SA/S0 protein contains an unmodeled C-terminal extension (~90 residues) that is specific to eukaryotes. This C-terminal extension could form a long α helix that is visible in the S-III protein density. Sufficient residues are also present to form a small domain with four helices at the end of the long α helix. This small helical domain sits on h40, contacts h38, and binds to RACK1. This positioning of the helical domain would not interfere with binding partners, such as the SRC and protein C kinases, which could bind to the top and lateral surfaces of the RACK1 β propeller (Sengupta et al., 2004).

Intersubunit Bridges

Ribosomes undergo a ratchet-like subunit rearrangement (RSR) during translation that involves a rotation of the small subunit relative to the large subunit (Figure 7A; Frank and Agrawal, 2000; Valle et al., 2003b; Spahn et al., 2004a). This process is coupled with an inward rotation of the head toward the E site (Figure 7A; Spahn et al., 2004a; Schuwirth et al., 2005; Berk and Cate, 2007). During the RSR, many intersubunit bridges must rearrange locally or be transiently broken (Gao et al., 2003; Spahn et al., 2004a). The origin for the ratcheting motion of the small subunit is near bridge 2c (b2c). This rotation displaces distal regions of $ES3^S$ and $ES6^S$ in the small subunit by ~20 Å. In addition, the exact nature of some bridges is dependent upon the conformation of the ribosome (Spahn et al., 2004a). To place our model in context with previous structures, we identified intersubunit bridges (Figure S11; Table S5). Interestingly, we found that bridges in our model are similar to those observed in a yeast ribosome without tRNAs (Spahn et al., 2004a), as exemplified by bridge 6 (b6), which forms a link between h14 and L23e (not shown).

We now describe bridges of particular interest in the canine ribosome. First, we observed a novel bridge (b3b) between h44 and H64 with a spacing of ~4.9 Å (Figure S11; Table S5). Very strong density for this feature suggests the possibility of an unusual RNA conformation in this region, as there are no proteins which could contribute to this bridge. As expected, bridges specific to eukaryotes are located along the platform side of the small subunit and are also present beneath this subunit (Figure 7A; Figure S11; Spahn et al., 2004a). As shown in Figure 7B, eukaryotic bridges (eb) 9, 12, and 11 are nearly contiguous. In addition, bridge 2e is positioned between eb8 and eb9. This link has a novel extension of the short C-terminal α helix of L37ae which extends toward h22. This flattened density may correspond to a β hairpin or an ordered loop (Figure 7C).

Many of the eukaryotic bridges involve expansion segments, novel proteins, or extensions of a conserved protein. For example, eb8 is formed by an extended feature in the novel S-IV protein. The actual bridge is composed of two helices with a kink between them which connects h23 with H79 on the large subunit. In addition, a possible extension of L7ae and ES31 may help form eb8 (Figure 7D). We also found a new bridge near eb8 (denoted eb8b) that links h23 and H76 (Figure S11). Another bridge (eb9) is formed by S13e and L30e and was described previously in a plant ribosome (Halic et al., 2005). In eb9, the N-terminal α helix of S13e is flipped outward by ~180° at the subunit interface and interacts with the novel protein S-IX (Figure 7E). A weak contact may also be present between h11 and H63 to form eb10 (not shown). Another bridge (eb11) is formed by a novel protein S-VII, which makes contacts with h9 and $ES3^S$ in the small subunit and ES41 in the large subunit (Figure 7F). Finally, eb12 is formed by a remarkable α helix that extends from the C terminus of L19e. This α helix spans a distance of ~40 Å as it crosses the subunit interface and interacts with a branch of $ES6^S$ in the small subunit (Figure 7G). Notably, the L19e extension is present in a map of the yeast ribosome (Schuler et al., 2006) and, thus, is probably conserved in all metazoans.

The actual functions of the novel eukaryotic bridges are not known, but a clue to their role may lie in the distribution of these links on the side and bottom of the small subunit (Figures 7A and 7B). We propose that the eukaryotic bridges could provide a restoring force to counter the ratcheting motion of the small subunit that is powered by eEF2-mediated GTP hydrolysis (Figure 7A; Spahn et al., 2004a; Frank and Agrawal, 2000). Hence, these bridges would help reset the ribosome for the next round of protein synthesis. This "return phase" of the ratcheting cycle may be more difficult in higher eukaryotes, because of the positioning of expansion segments near the subunit interface. These segments include $ES3^S$, $ES6^S$, $ES12^S$, ES27, and ES41 (Figures

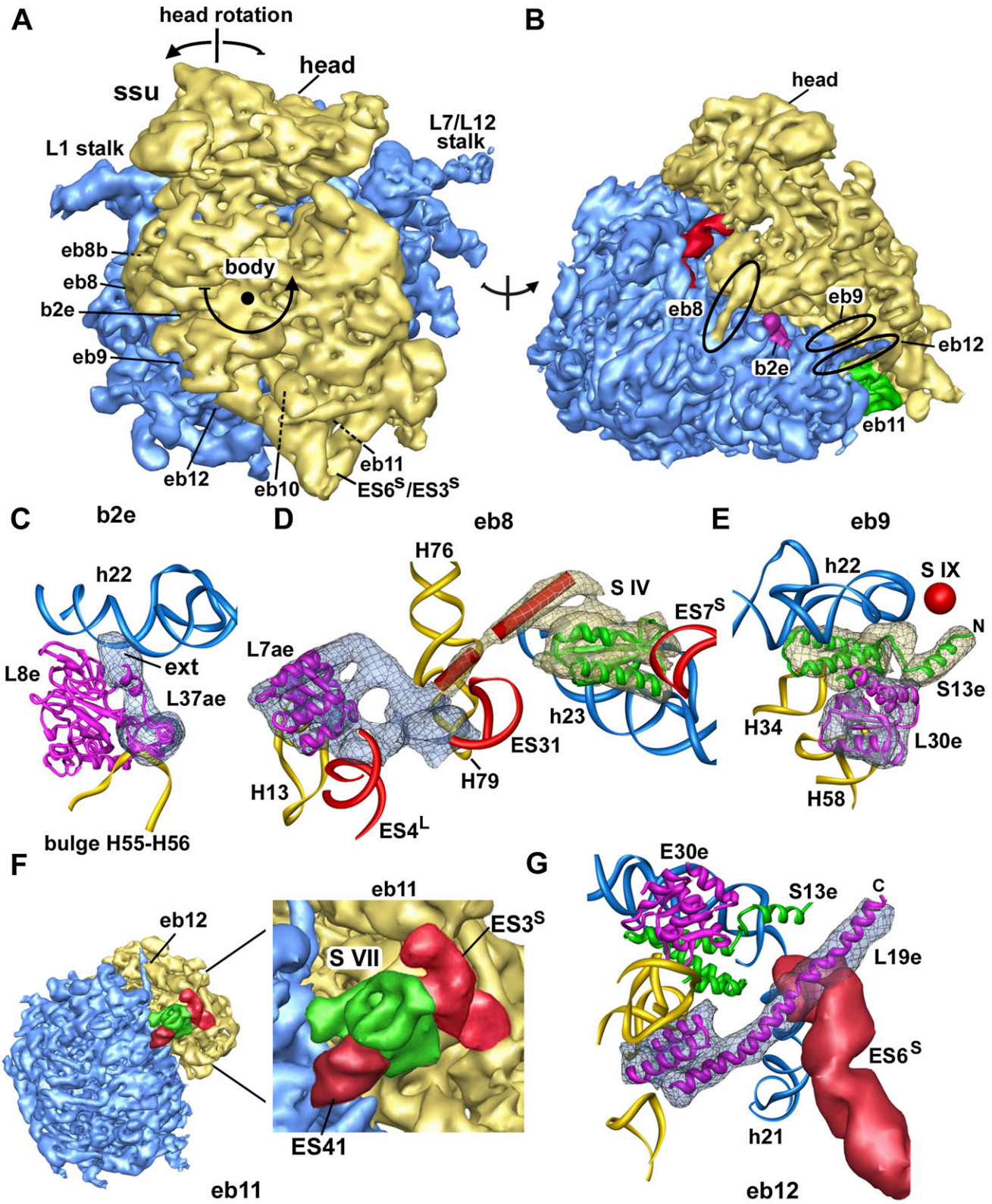

Figure 7. Intersubunit Bridges in the Canine Ribosome

(A) Known rotations of the body and head of the small subunit are indicated by arrows on the canine ribosome. Positions of the bridges specific to eukaryotic ribosomes and bridge 2e are indicated.

3A, 3B, and 3D). In fact, ES27 is the largest expansion segment (Figure S8B) and, even though it is flexible, ES27 could have a significant impact on this region of the ribosome.

Conformation of the Small Subunit

In the yeast ribosome, a latch is present between the head and shoulder of the small subunit. This latch helps form the mRNA entrance into the ribosome and may regulate mRNA access into the decoding center (Spahn et al., 2004a). A similar latch is present in our structure. This latch is formed by h34 and a loop of S3e in the head which are vertically aligned with h18 in the shoulder (Figures 8A and 8B). A similar latch was observed in a crystal structure of a programmed *Escherichia coli* ribosome (Berk et al., 2006). Remarkably, the position of the small and large subunits in this programmed *E. coli* ribosome are similar to those in our model of the canine ribosome, even though a P site tRNA is absent in our structure (not shown).

Because the core regions are structurally similar in all cytoplasmic ribosomes, the conformational changes that play a role in tRNA translocation should be conserved. To test this hypothesis, we aligned structures of 70S and 80S ribosomes using conserved regions of the large subunit. We first looked at the latch region in 80S ribosomes. A close-up of this region is shown for the canine ribosome with an E site tRNA (shown in blue, Figure 8C, left) and the yeast 80S-eEF2-sordarin complex (shown in red; Spahn et al., 2004a). This comparison shows that the head of the small subunit is quite dynamic, as proposed previously (Spahn et al., 2004a). Thus, the head may move from an open position, as seen in our model, to a closed conformation, like that seen in the yeast ribosome with eEF2 and sordarin (Spahn et al., 2004a). During this movement, the head would pivot toward the exit site through an angle of ~25° and h34 is displaced by ~22 Å.

The generality of this head movement is shown by a comparison of known 80S and 70S structures (Figure 8C, right). In this top view of the small subunit, known structures were placed in the order: 80S ribosome with E site tRNA (labeled C), 70S ribosome with A, P, and E site tRNAs (T; Selmer et al., 2006; Korostelev et al., 2006), conformer II of the *E. coli* ribosome (E-II; Schuwirth et al., 2005), and the yeast ribosome with eEF2 and sordarin (Y; Spahn et al., 2004a). Note that the S3e protein is shown only for the canine ribosome. Together, these 70S and 80S structures show a conserved movement of the head as it moves from an open to a closed position during the ratcheting of the small subunit.

DISCUSSION

In this paper, we have presented a molecular model of the canine 80S ribosome with an E site tRNA. Our model is based on a structure determined at ~8.7 Å resolution and provides insights into novel features of the eukaryotic ribosome. In particular, our structure lends support to current models in which the head of the small subunit and the L1 stalk play significant roles in tRNA translocation. We also characterized the eukaryotic intersubunit bridges. We propose that these novel intersubunit bridges may help restore the ribosome to an initial conformation with bound P and E site tRNAs, to prepare for the next cycle of chain elongation.

The Mammalian 80S Ribosome

We found that subunit rRNAs and conserved proteins in the mammalian ribosome are similar to their counterparts in bacterial and archaeal ribosomes, although numerous local variations have occurred during evolution. Eukaryotic ribosomes are much larger than their bacterial counterparts, as a result of the presence of rRNA expansion segments and novel proteins. The expansion segments and novel proteins are located on solvent-exposed regions of the subunits and a large amount of rRNA is positioned so that it faces the endoplasmic reticulum (ER) membrane. In addition, many conserved proteins and novel proteins bind to expansion segments and stabilize their packing on the ribosome. Thus, expansion segments and novel proteins appear to have coevolved as an integrated framework that envelopes the conserved core of the cytoplasmic ribosome without impeding its function.

In general, little is known about the function of expansion segments. However, a large expansion segment is required for cell viability (ES27; Sweeney et al., 1994). Expansion segments could play a role in subunit assembly within the nucleolus or they may stabilize the mature ribosome (Sweeney et al., 1994). In addition, expansion segments could facilitate certain aspects of translation (Gao et al., 2005). Indeed, some expansion segments could act as a negatively charged sink to recruit positively charged factors to the ribosome. In another scenario, expansion segments may help target the ribosome to cytoplasmic sites within the larger eukaryotic cell.

Novel proteins interact with expansion segments or conserved subunit rRNAs in the eukaryotic ribosome. Thus, it is striking that ordered density has been found for only 20 of the novel proteins (out of 31; also see Spahn et al., 2001, 2004a). There are a number of possible reasons for this discrepancy. Some novel proteins could be present at low occupancy or they may be lost during purification. In addition, some novel proteins could interact with flexible regions of the ribosome, and thus would go undetected in our 3D map. The energy burden of synthesizing novel proteins and expansion segments, coupled with their ubiquitous presence in eukaryotes, suggests that these components must play an important role in ribosome biology. Therefore, it seems likely that additional processes will be discovered which use these novel components of the 80S ribosome.

In this work, we also showed that RACK1 associates with the head of the small subunit and has multiple binding sites that involve rRNA and novel protein contacts. These interactions

(B) A reverse view of the ribosome shows that the ebs form a contiguous line along the lateral edge of the small subunit and are also present beneath the subunits (eb11).
(C) An unmodeled C-terminal extension of L37ae contacts h22 in bridge 2e.
(D) An α helix originates from S-IV and extends across the subunit interface to form eb8. Additional density from L7ae and ES31 helps to form this bridge near the L1 stalk helix (H76).
(E) Bridge 9 (eb9) involves extensive interactions between L30e and S13e. The N-terminal helix of S13e is flipped out to interact with protein S-IX.
(F) Protein S-VII forms a bridge between $ES3^S$ and ES41. An icon view in the lower left shows the proximity of eb11 and eb12.
(G) A C-terminal extension of L19e forms a long helix that crosses the intersubunit gap to interact with one branch of $ES6^S$.

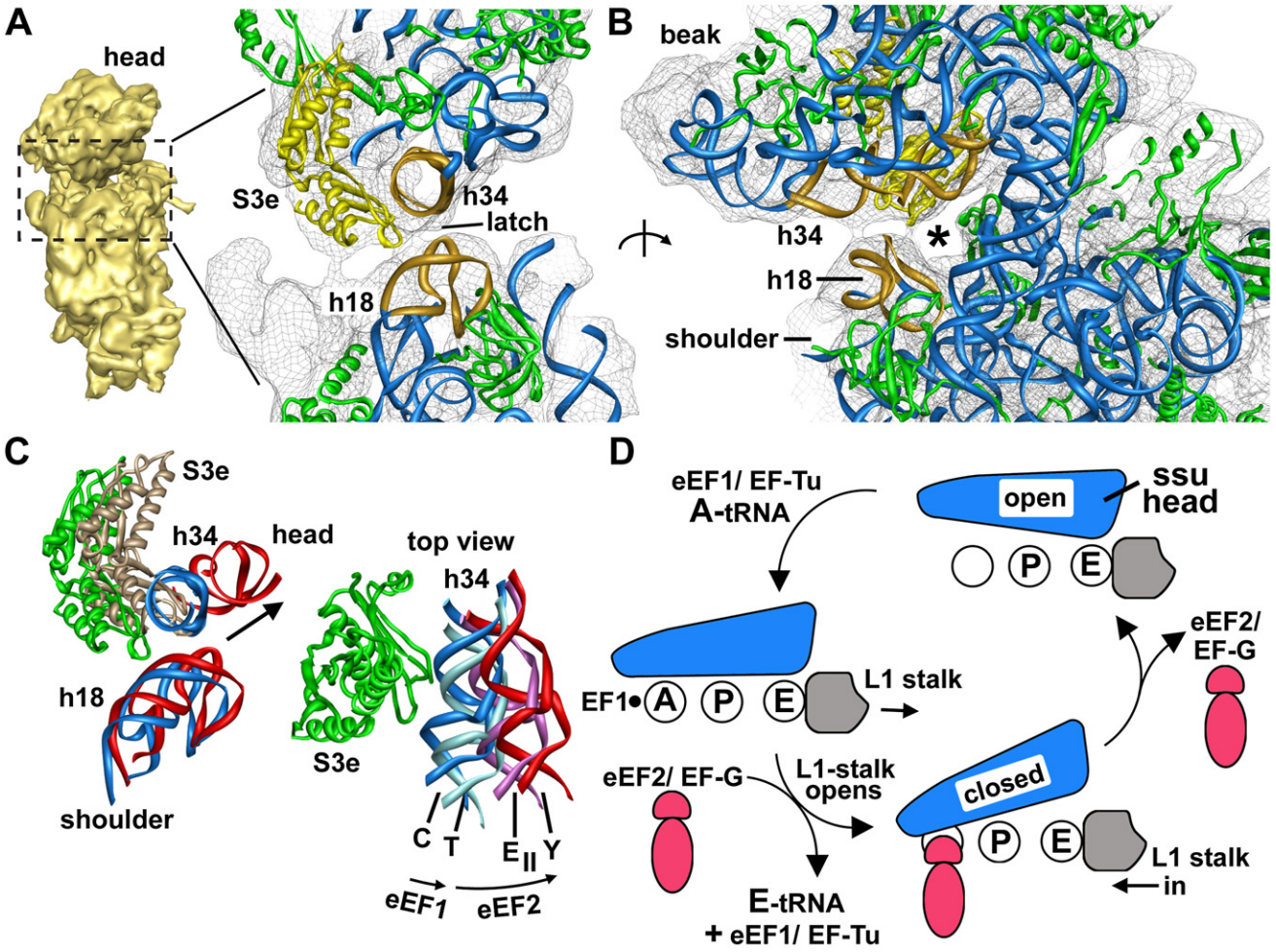

Figure 8. Conformational Changes of the Small Subunit

(A) A latch is present between H34 and S3e in the head of the ssu and h18 in the shoulder. The helices are shown in gold and S3e is in yellow.

(B) The head of the ssu is rotated ~90° clockwise to show the latch and the mRNA entrance channel (marked with an asterisk).

(C) Left: a comparison between the canine ribosome with an E site tRNA (rRNA, blue; S3e, green) and a yeast model with bound eEF2-sordarin (rRNA, red; S3e, tan) reveals a large rotation of the head relative to h18 in the shoulder. Right: a top view reveals a hypothetical, progressive rotation series for the head of the ssu. The h34 helices are color coded as above, with the cyan h34 from a programmed *Thermus* ribosome (PDB code: 2j00) and the pink h34 from the second conformational model of an *E. coli* ribosome (PDB code: 2aw7).

(D) A general model is shown for head rotation in the ssu and movements of the L1 stalk during the translation cycle.

leave the top and lateral surfaces of RACK1 unencumbered, so the receptor may bind to partners that regulate initiation and translation (Sengupta et al., 2004; Nilsson et al., 2004). Because RACK1 is found in plant, yeast, and animal ribosomes, it appears that this kinase C receptor is an intrinsic component of eukaryotic ribosomes (Chang et al., 2005; Sengupta et al., 2004; this work).

Rearrangements during Translation

The sequential actions of eEF1 and eEF2 introduce a cognate amino-acylated tRNA into the A site and then move this tRNA into the P site during peptide bond formation. During this process, the small subunit undergoes a ratcheting motion relative to the large subunit and the head moves toward the E site (Frank and Agrawal, 2000; Valle et al., 2003b; Spahn et al., 2004a). Within the framework of this model, our structure provides further support for the idea that the head may pivot from an open to a more closed conformation during the translation cycle (Spahn et al., 2004a; Schuwirth et al., 2005). The magnitude of the observed head movements (~20 Å) suggests that this process may facilitate the lateral translocation of tRNAs (Spahn et al., 2004a; Schuwirth et al., 2005; Berk and Cate, 2007).

As summarized in Figure 8D, the transition from a ribosome with bound P and E site tRNAs and an open head conformation to a ribosome with three occupied tRNA sites is catalyzed by eEF1. This would involve a small rotation of the head toward the closed position and local changes around h18 to accommodate tRNA binding in the A site (Figure 8D, left). After dissociation of eEF1, the binding of eEF2 displaces the A site tRNA into the P site, with a further rotation of the head toward the E site. Lateral movements of tRNAs during this process would induce the L1 stalk to open with a concomitant release of the E site tRNA. This release is facilitated by eEF3 in fungi (Andersen et al.,

2006). In mammals, the release of an E site tRNA may involve the uncoupling of a novel α-helical connection between a large subunit protein and the L1 stalk. After the E site tRNA is released, the L1 stalk could bind to a deacylated tRNA as it moves into the vacant E site from the P site (Figure 8D, bottom). Finally, release of eEF2 would allow the head to swivel back to its open position (Figure 8D, top) as the body of the small subunit pivots back to its original position to complete the ratcheting motion. This "head" cycle appears to be conserved in 70S and 80S ribosomes as part of the ratcheting motion of the small subunit. During this cycle, the L1 stalk may adopt at least two different conformations.

The intersubunit bridges may play a significant role in modulating movements of the small subunit. We find that bridges specific to eukaryotic ribosomes are formed by novel proteins, expansion segments in rRNA, and insertions in conserved ribosomal proteins. These links are present along the platform side of the small subunit and two additional bridges are located near the bottom of the small subunit. Two of the bridges (eb8 and eb12) use α helices to span the gap between the subunits. We suggest that the novel eukaryotic bridges may facilitate the return motion of the small subunit during the ratchet-like movement. Although eEF2 drives the forward direction of the small subunit during its ratcheting motion, numerous expansion segments near the subunit interface may form an impediment to the small subunit which must return to its original position to complete the cycle. Thus, the eukaryotic bridges may set the stage for further chain elongation by helping to restore the ribosome to an initial conformation with bound P and E site tRNAs that is ready to accept incoming acyl-tRNAs.

EXPERIMENTAL PROCEDURES

Please see the Supplemental Experimental Procedures.

ACCESSION NUMBERS

The ribosome map and coordinates for the 80S model have been deposited in the EMD and RCSB under accession numbers EMD1480, 2ZKQ, and 2ZKR.

SUPPLEMENTAL DATA

Supplemental Data include eleven figures, five tables, Supplemental Experimental Procedures, and Supplemental References and can be found with this article online at http://www.structure.org/cgi/content/full/16/4/535/DC1/.

ACKNOWLEDGMENTS

We thank A. Neuhof for preparation of the canine RCC samples, T.A. Rapoport for his continued support, F. Fabiola, A. Korostelev, and M.S. Chapmann for discussions on CNS-RSREF, B. Webb for help with MODELLER, and T.D. Goddard for help with Chimera. We also thank S.J. Ludtke for suggesting the use of the sep option in EMAN. This work was supported by grants to R.R.G. (GM067317), A.S. (NIH R01 GM54762, NIH PN2 EY016525, and NSF IIS-0705196), and C.W.A. (NIH RO1 GM45377). A.S. also acknowledges support from the Sandler Family Supporting Foundation, Hewlett-Packard, NetApps, IBM, and Intel. M.T. is supported by an MRC Career Development Award.

Received: October 29, 2007
Revised: January 3, 2008
Accepted: January 26, 2008
Published: April 8, 2008

REFERENCES

Allen, G.S., Zavialov, A., Gursky, R., Ehrenberg, M., and Frank, J. (2005). The cryo-EM structure of a translation initiation complex from *Escherichia coli*. Cell *121*, 703–712.

Andersen, C.B., Becker, T., Blau, M., Anand, M., Halic, M., Balar, B., Mielke, T., Boesen, T., Pedersen, J.S., Spahn, C.M., et al. (2006). Structure of eEF3 and the mechanism of transfer RNA release from the E-site. Nature *443*, 663–668.

Ban, N., Nissen, P., Hansen, J., Moore, P.B., and Steitz, T.A. (2000). The complete atomic structure of the large ribosomal subunit at 2.4 Å resolution. Science *289*, 905–920.

Beckmann, R., Spahn, C.M., Eswar, N., Helmers, J., Penczek, P.A., Sali, A., Frank, J., and Blobel, G. (2001). Architecture of the protein-conducting channel associated with the translating 80S ribosome. Cell *107*, 361–372.

Berk, V., and Cate, J.H. (2007). Insights into protein biosynthesis from structures of bacterial ribosomes. Curr. Opin. Struct. Biol. *17*, 302–309.

Berk, V., Zhang, W., Pai, R.D., and Cate, J.H. (2006). Structural basis for mRNA and tRNA positioning on the ribosome. Proc. Natl. Acad. Sci. USA *103*, 15830–15834.

Brodersen, D.E., Clemons, W.M., Jr., Carter, A.P., Morgan-Warren, R.J., Wimberly, B.T., and Ramakrishnan, V. (2000). The structural basis for the action of the antibiotics tetracycline, pactamycin, and hygromycin B on the 30S ribosomal subunit. Cell *103*, 1143–1154.

Carter, A.P., Clemons, W.M., Brodersen, D.E., Morgan-Warren, R.J., Wimberly, B.T., and Ramakrishnan, V. (2000). Functional insights from the structure of the 30S ribosomal subunit and its interactions with antibiotics. Nature *407*, 340–348.

Ceci, M., Gaviraghi, C., Gorrini, C., Sala, L.A., Offenhauser, N., Marchisio, P.C., and Biffo, S. (2003). Release of eIF6 (p27BBP) from the 60S subunit allows 80S ribosome assembly. Nature *426*, 579–584.

Chang, I.F., Szick-Miranda, K., Pan, S., and Bailey-Serres, J. (2005). Proteomic characterization of evolutionarily conserved and variable proteins of *Arabidopsis* cytosolic ribosomes. Plant Physiol. *137*, 848–862.

Datta, P.P., Sharma, M.R., Qi, L., Frank, J., and Agrawal, R.K. (2005). Interaction of the G′ domain of elongation factor G and the C-terminal domain of ribosomal protein L7/L12 during translocation as revealed by cryo-EM. Mol. Cell *20*, 723–731.

Diaconu, M., Kothe, U., Schlunzen, F., Fischer, N., Harms, J.M., Tonevitsky, A.G., Stark, H., Rodnina, M.V., and Wahl, M.C. (2005). Structural basis for the function of the ribosomal L7/12 stalk in factor binding and GTPase activation. Cell *121*, 991–1004.

Dresios, J., Panopoulos, P., and Synetos, D. (2006). Eukaryotic ribosomal proteins lacking a eubacterial counterpart: important players in ribosomal function. Mol. Microbiol. *59*, 1651–1663.

Dube, P., Bacher, G., Stark, H., Mueller, F., Zemlin, F., van Heel, M., and Brimacombe, R. (1998). Correlation of the expansion segments in mammalian rRNA with the fine structure of the 80S ribosome: a cryo-electron microscopic reconstruction of the rabbit reticulocyte ribosome at 21 Å resolution. J. Mol. Biol. *279*, 403–421.

Frank, J., and Agrawal, R.K. (2000). A ratchet-like inter-subunit reorganization of the ribosome during translocation. Nature *406*, 318–322.

Frank, J., Sengupta, J., Gao, H., Li, W., Valle, M., Zavialov, A., and Ehrenberg, M. (2005). The role of tRNA as a molecular spring in decoding, accommodation, and peptidyl transfer. FEBS Lett. *579*, 959–962.

Fromont-Racine, M., Senger, B., Saveanu, C., and Fasiolo, F. (2003). Ribosome assembly in eukaryotes. Gene *313*, 17–42.

Gao, H., Sengupta, J., Valle, M., Korostelev, A., Eswar, N., Stagg, S.M., Van Roey, P., Agrawal, R.K., Harvey, S.C., Sali, A., et al. (2003). Study of the structural dynamics of the *E. coli* 70S ribosome using real-space refinement. Cell *113*, 789–801.

Gao, H., Ayub, M.J., Levin, M.J., and Frank, J. (2005). The structure of the 80S ribosome from *Trypanosoma cruzi* reveals unique rRNA components. Proc. Natl. Acad. Sci. USA *102*, 10206–10210.

Gerbi, S.A. (1996). Expansion segments: regions of variable size that interrupt the universal core secondary structure of ribosomal RNA. In Ribosomal RNA, Structure, Evolution, Processing, and Function in Protein Biosynthesis, R.A. Zimmermann and A.E. Dahlberg, eds. (New York: CRC Press), pp. 71–87.

Goddard, T.D., Huang, C.C., and Ferrin, T.E. (2005). Software extensions to UCSF Chimera for interactive visualization of large molecular assemblies. Structure *13*, 473–482.

Gomez-Lorenzo, M.G., Spahn, C.M., Agrawal, R.K., Grassucci, R.A., Penczek, P., Chakraburtty, K., Ballesta, J.P., Lavandera, J.L., Garcia-Bustos, J.F., and Frank, J. (2000). Three-dimensional cryo-electron microscopy localization of EF2 in the *Saccharomyces cerevisiae* 80S ribosome at 17.5 Å resolution. EMBO J. *19*, 2710–2718.

Gonzalo, P., and Reboud, J.P. (2003). The puzzling lateral flexible stalk of the ribosome. Biol. Cell *95*, 179–193.

Green, R., and Noller, H.F. (1997). Ribosomes and translation. Annu. Rev. Biochem. *66*, 679–716.

Halic, M., Becker, T., Frank, J., Spahn, C.M., and Beckmann, R. (2005). Localization and dynamic behavior of ribosomal protein L30e. Nat. Struct. Mol. Biol. *12*, 467–468.

Harms, J., Schluenzen, F., Zarivach, R., Bashan, A., Gat, S., Agmon, I., Bartels, H., Franceschi, F., and Yonath, A. (2001). High resolution structure of the large ribosomal subunit from a mesophilic eubacterium. Cell *107*, 679–688.

Jenni, S., and Ban, N. (2003). The chemistry of protein synthesis and voyage through the ribosomal tunnel. Curr. Opin. Struct. Biol. *13*, 212–219.

Korostelev, A., Trakhanov, S., Laurberg, M., and Noller, H.F. (2006). Crystal structure of a 70S ribosome-tRNA complex reveals functional interactions and rearrangements. Cell *126*, 1065–1077.

Ludtke, S.J., Baldwin, P.R., and Chiu, W. (1999). EMAN: semiautomated software for high-resolution single-particle reconstructions. J. Struct. Biol. *128*, 82–97.

Ménétret, J.F., Hegde, R.S., Heinrich, S., Chandramouli, P., Ludtke, S.J., Rapoport, T.A., and Akey, C.W. (2005). Architecture of the ribosome-channel complex derived from native membranes. J. Mol. Biol. *348*, 445–457.

Morgan, D.G., Ménétret, J.F., Neuhof, A., Rapoport, T.A., and Akey, C.W. (2002). Structure of the mammalian ribosome-channel complex at 17Å resolution. J. Mol. Biol. *324*, 871–886.

Nilsson, J., Sengupta, J., Frank, J., and Nissen, P. (2004). Regulation of eukaryotic translation by the RACK1 protein: a platform for signalling molecules on the ribosome. EMBO Rep. *5*, 1137–1141.

Ogle, J.M., and Ramakrishnan, V. (2005). Structural insights into translational fidelity. Annu. Rev. Biochem. *74*, 129–177.

Ogle, J.M., Brodersen, D.E., Clemons, W.M., Jr., Tarry, M.J., Carter, A.P., and Ramakrishnan, V. (2001). Recognition of cognate transfer RNA by the 30S ribosomal subunit. Science *292*, 897–902.

Pioletti, M., Schlunzen, F., Harms, J., Zarivach, R., Gluhmann, M., Avila, H., Bashan, A., Bartels, H., Auerbach, T., Jacobi, C., et al. (2001). Crystal structures of complexes of the small ribosomal subunit with tetracycline, edeine and IF3. EMBO J. *20*, 1829–1839.

Ramakrishnan, V. (2002). Ribosome structure and the mechanism of translation. Cell *108*, 557–572.

Rudra, D., and Warner, J.R. (2004). What better measure than ribosome synthesis? Genes Dev. *18*, 2431–2436.

Schluenzen, F., Tocilj, A., Zarivach, R., Harms, J., Gluhmann, M., Janeli, D., Bashan, A., Bartels, H., Agmon, I., Franceschi, F., et al. (2000). Structure of functionally activated small ribosomal subunit at 3.3 Å resolution. Cell *102*, 615–623.

Schmeing, T.M., Huang, K.S., Strobel, S.A., and Steitz, T.A. (2005). An induced-fit mechanism to promote peptide bond formation and exclude hydrolysis of peptidyl-tRNA. Nature *438*, 520–524.

Schnare, M.N., Damberger, S.H., Gray, M.W., and Gutell, R.R. (1996). Comprehensive comparison of structural characteristics in eukaryotic cytoplasmic large subunit (23S-like) ribosomal RNA. J. Mol. Biol. *256*, 701–719.

Schuler, M., Connell, S.R., Lescoute, A., Giesebrecht, J., Dabrowski, M., Schroeer, B., Mielke, T., Penczek, P.A., Westhof, E., and Spahn, C.M. (2006). Structure of the ribosome-bound cricket paralysis virus IRES RNA. Nat. Struct. Mol. Biol. *13*, 1092–1096.

Schuwirth, B.S., Borovinskaya, M.A., Hau, C.W., Zhang, W., Vila-Sanjurjo, A., Holton, J.M., and Cate, J.H. (2005). Structures of the bacterial ribosome at 3.5 Å resolution. Science *310*, 827–834.

Selmer, M., Dunham, C.M., Murphy, F.V., IV, Weixlbaumer, A., Petry, S., Kelley, A.C., Weir, J.R., and Ramakrishnan, V. (2006). Structure of the 70S ribosome complexed with mRNA and tRNA. Science *313*, 1935–1942.

Sengupta, J., Nilsson, J., Gursky, R., Spahn, C.M., Nissen, P., and Frank, J. (2004). Identification of the versatile scaffold protein RACK1 on the eukaryotic ribosome by cryo-EM. Nat. Struct. Mol. Biol. *11*, 957–962.

Spahn, C.M., Beckmann, R., Eswar, N., Penczek, P.A., Sali, A., Blobel, G., and Frank, J. (2001). Structure of the 80S ribosome from *Saccharomyces cerevisiae*—tRNA-ribosome and subunit-subunit interactions. Cell *107*, 373–386.

Spahn, C.M., Gomez-Lorenzo, M.G., Grassucci, R.A., Jorgensen, R., Andersen, G.R., Beckmann, R., Penczek, P.A., Ballesta, J.P., and Frank, J. (2004a). Domain movements of elongation factor eEF2 and the eukaryotic 80S ribosome facilitate tRNA translocation. EMBO J. *23*, 1008–1019.

Spahn, C.M., Jan, E., Mulder, A., Grassucci, R.A., Sarnow, P., and Frank, J. (2004b). Cryo-EM visualization of a viral internal ribosome entry site bound to human ribosomes: the IRES functions as an RNA-based translation factor. Cell *118*, 465–475.

Stark, H., Rodnina, M.V., Wieden, H.J., van Heel, M., and Wintermeyer, W. (2000). Large-scale movement of elongation factor G and extensive conformational change of the ribosome during translocation. Cell *100*, 301–309.

Stark, H., Rodnina, M.V., Wieden, H.J., Zemlin, F., Wintermeyer, W., and van Heel, M. (2002). Ribosome interactions of aminoacyl-tRNA and elongation factor Tu in the codon-recognition complex. Nat. Struct. Biol. *9*, 849–854.

Sweeney, R., Chen, L., and Yao, M.C. (1994). An rRNA variable region has an evolutionarily conserved essential role despite sequence divergence. Mol. Cell. Biol. *14*, 4203–4215.

ter Haar, E., Musacchio, A., Harrison, S.C., and Kirchhausen, T. (1998). Atomic structure of clathrin: a β propeller terminal domain joins an α zigzag linker. Cell *95*, 563–573.

Topf, M., Baker, M.L., Marti-Renom, M.A., Chiu, W., and Sali, A. (2006). Refinement of protein structures by iterative comparative modeling and cryoEM density fitting. J. Mol. Biol. *357*, 1655–1668.

Topf, M., Lasker, K., Webb, B., Wolfson, H., Chiu, W., and Sali, A. (2008). Protein structure fitting and refinement guided by cryo-EM density. Structure *16*, 295–307.

Valle, M., Zavialov, A., Li, W., Stagg, S.M., Sengupta, J., Nielsen, R.C., Nissen, P., Harvey, S.C., Ehrenberg, M., and Frank, J. (2003a). Incorporation of aminoacyl-tRNA into the ribosome as seen by cryo-electron microscopy. Nat. Struct. Biol. *10*, 899–906.

Valle, M., Zavialov, A., Sengupta, J., Rawat, U., Ehrenberg, M., and Frank, J. (2003b). Locking and unlocking of ribosomal motions. Cell *114*, 123–134.

Wimberly, B.T., Brodersen, D.E., Clemons, W.M., Jr., Morgan-Warren, R.J., Carter, A.P., von Rhein, C., Hartsch, T., and Ramakrishnan, V. (2000). Structure of the 30S ribosomal subunit. Nature *407*, 327–339.

Wool, I.G., Chan, Y.L., and Gluck, A. (1995). Structure and evolution of mammalian ribosomal proteins. Biochem. Cell Biol. *73*, 933–947.

Yusupov, M.M., Yusupova, G.Z., Baucom, A., Lieberman, K., Earnest, T.N., Cate, J.H., and Noller, H.F. (2001). Crystal structure of the ribosome at 5.5 Å resolution. Science *292*, 883–896.

Yusupova, G.Z., Yusupov, M.M., Cate, J.H., and Noller, H.F. (2001). The path of messenger RNA through the ribosome. Cell *106*, 233–241.

Yusupova, G., Jenner, L., Rees, B., Moras, D., and Yusupov, M. (2006). Structural basis for messenger RNA movement on the ribosome. Nature *444*, 391–394.

